Histological and behavioural phenotypes of a novel mutated *APP* knock-in mouse

Kaja Plucińska[1], Barry Crouch, Jie M Yeap, Sandra Stoppelkamp[2], Gernot Riedel, Bettina Platt*

School of Medicine, Medical Sciences & Nutrition
University of Aberdeen,
Aberdeen AB25 2ZD, UK

[1] *Present address: The Novo Nordisk Foundation Centre for Basic Metabolic Research, Section for Integrative Physiology, University of Copenhagen, Copenhagen 2100 N, Denmark*

[2] *Present address: Clinical Research Laboratory, Department of Thoracic, Cardiac and Vascular Surgery, University Hospital Tübingen, Tübingen University, Calwerstr. 7/1, 72076 Tübingen, Germany*

* Corresponding author:
Prof. Bettina Platt, PhD
Chair in Translational Neuroscience
School of Medicine, Medical Sciences & Nutrition
University of Aberdeen
Foresterhill
ABERDEEN AB25 2ZD
Scotland, UK
Tel.: (+44) 1224 437402
FAX: (+44) 1224 437465

RUNNING TITLE: Behaviour and histology in a novel *APP* knock-in mouse

ABSTRACT

Gene mutations within Amyloid Precursor Protein (*APP* or *AβPP*) and/or Presenilin 1 (*PS1*) are determinant of familial Alzheimer's disease (fAD) and remain fundamental for experimental models. Here, we generated a neuronal knock-in mouse ($PLB2_{APP}$) with mutated human $APP^{Swe/Lon}$ and investigated histopathology and behavioural changes. Additionally, $PLB2_{APP}$ mice were cross-bred with a presenilin ($PS1^{A246E}$) line to assess the impact of this risk gene combination in mice.

Immunohistochemistry determined Aβ-pathology, astrogliosis (via GFAP labelling) and neuronal densities in hippocampal and cortical brain regions. One-year old $PLB2_{APP}$ mice showed higher levels of intracellular Aβ in CA1, dentate gyrus and cortical regions compared to PLB_{WT} controls. Co-expression of *PS1* reduced hippocampal but elevated cortical build-up of soluble and fibrillar Aβ. Amyloid plaques were sparse in aged $PLB2_{APP}$ mice, co-expression of *PS1* promoted plaque formation. Heightened GFAP expression followed the region-specific pattern of Aβ in $PLB2_{APP}$ and $PLB2_{APP/PS1}$ mice. Behaviourally, habituation to a novel environment, circadian activity and spatial reference memory were assessed at 6 and 12 months. Habituation was delayed in 6-month old $PLB2_{APP}$ mice, and overall home-cage activity was reduced in both lines at 6 and 12 months, particularly during the dark phase. Spatial learning in the water maze task was impaired in $PLB2_{APP}$ mice independent of *PS1* expression; this was associated with a reduced employment of spatial navigation strategies. Memory retrieval was compromised in $PLB2_{APP}$ mice only.

Our data demonstrate that low expression of *APP* is sufficient to drive histopathological and cognitive changes in mice without over-expression or excessive plaque deposition. AD-like phenotypes were altered by co-expression of *PS1*, including a shift from hippocampal to cortical Aβ pathology, alongside reduced deficits in spatial learning.

KEYWORDS: *amyloid, inflammation, habituation, cognition, spatial learning, search strategies*

INTRODUCTION

Mutations of the Amyloid Precursor Protein (*APP* or *AβPP*) and Presenilin 1 (*PS1*) genes linked with familial Alzheimer's disease (fAD) have greatly influenced our understanding of disease pathology. Beta-Amyloid is produced via abnormal proteolysis of AβPP by β-secretase (BACE1) and γ-secretases (with PS1 as an essential component) and readily forms assemblies such as oligomers and amyloid plaques typical for AD-afflicted brains [1]. Although AD is an overwhelmingly sporadic and heterogeneous condition characterised by complex neuronal histopathology, genetic mutations within *APP* and *PS1* continue to guide experimental modelling of AD-associated amyloidosis in mice. The majority of mouse models generated to date relied on random transgene insertion and overexpression, and hence their relevance for the human condition has been questioned [2]. To address this issue, we generated and characterized several knock-in mouse models expressing either multiple dementia-relevant mutated genes such as human *APP*, *TAU* and *PS1* ($PLB1_{Triple}$ mouse) [3-5], single gene knock-in lines expressing human *BACE1* (termed PLB4) [6,7], or human mutant *TAU* ($PLB2_{TAU}$) [8]. In contrast to the conventional AD mouse models, PLB knock-in mice have a low expression of human AD genes, controlled by CaMKIIα promoter ensuring neuronal specificity. The phenotypes observed in PLB lines demonstrated for the first time that low levels and neuron-specific expression dementia relevant genes is sufficient to drive neuropathological events as well as cognitive phenotypes typical for either sporadic AD ($PLB4_{BACE1}$ mice), fAD ($PLB1_{Triple}$ mice) or frontotemporal dementia ($PLB2_{TAU}$). Due to the identical background and insertion locus, a direct comparisons between the 3 mouse models has allowed us to carefully dissect the relationships between the genetic components, defined pathologies and behavioural phenotypes; e.g. amyloid-driven hippocampal pathology resulted in spatial learning impairments in the $PLB1_{Triple}$ and BACE1 mice [3-6], while $PLB2_{TAU}$ mice showed frontal pathologies associated with altered semantic memory and cognitive flexibility [8].

Here, we aimed to investigate whether neuronal expression of a single mutated human *AβPP* gene (carrying *Swedish* and *London* mutations: K670N, M671L, V717I) was sufficient to induce amyloidosis and behavioural changes in mice (termed $PLB2_{APP}$), following on from our previously reported $PLB1_{Triple}$ model carrying the same *APP* transgene. We also set out to assess the effects of mutant *PS1* (A246E) co-expression (double-transgenic $PLB2_{APP/PS1}$) on histological and cognitive profiles, also part of the genetic make-up of the $PLB1_{Triple}$ line.

Several single-transgenic (over-expression) *AβPP* mice have been generated to date with various fAD genes, mutations and promoters such as platelet-derived growth factor-β (PDGF-β), prion protein (PrP) and Thy1. These first generation models included the PDAPP [9,10], Tg2576 [11], APP23 [12], J20 [13] and TgCRND8 [14], harbouring either 695 or 770 *APP* gene constructs

with one or more mutations. The most commonly used *Swedish* K670N/M671L mutation [15] induces overproduction of Aβ from AβPP, accelerating extracellular Aβ deposition. The *London* mutation V717l is associated with an increased $A\beta_{42}/A\beta_{40}$ ratio by increasing $A\beta_{42}$ levels and little or no effect on the $A\beta_{40}$ levels [16-18]. The V717l mutation is also linked to altered APP subcellular localization, soluble APP-β (sAPP-β) generation, as well as tau expression and phosphorylation. Transgenic mice carrying the *Swedish* and/or *London* mutations were reported to develop cognitive dysfunction from ~3 months of age coinciding with excessive $A\beta_{42}$ accumulation and plaque deposition across different brain regions, partially mimicking age-associated AD pathology [2].

In an attempt to re-create the pathological hallmarks of AD several groups generated transgenic mice overexpressing human mutated *PS1* gene. Although *PS1* mutations cause the majority of early-onset fAD cases [19], overexpression or knock-in of mutant *PS1* alone did not induce Aβ pathology in mice [20-22]. This lack of amyloidosis was attributed to insufficient levels of $A\beta_{42}$ or $A\beta_{43}$ fragments from mouse APP protein, and its lower amyloidogenic potential due to a difference in three amino acids compared to human Aβ. Thereafter, genetic crosses such as Tg2576 and $PS1_{M146L}$Tg [23], $APP_{KM679/671NL}$Tg and $PS1_{A246E}$Tg [24], $APP_{KM670/671NL\text{-}V717l}$ and $PS1^{M233T/L23P}$ knock-in [25] demonstrated that co-expression of *PS1* mutations in human *AβPP* transgenic mice accelerates cerebral Aβ deposition, gliosis and the symptomatic age to as early as 1 or 2 months. These studies have substantially influenced the way we understand the role of *AβPP* and *PS1* gene mutations in the pathogenic events in fAD, particularly concerning the production of specific Aβ species. However, they also ultimately raised a genuine concern about their disease-relevant face validity in relation to the human condition: neuropathological and behavioural changes emerged during development, resulting in a rather tenuous translation to the age-related symptom progression observed in human AD, and behavioural phenotypes vs amyloid load often did not correlate [5]. Hence, new generation AD models are now sought to allow for dissecting Aβ pathology and cognitive phenotypes without artefacts and phenotypes induced by overexpression of the *AβPP* gene.

Recent developments have addressed some of the drawbacks associated with the first generation AD models, through the use of novel tools for genetic manipulation such as the knock-in strategies. Similarly to PLB lines, recent reports demonstrate that *App* knock-in [26], where the murine Aβ sequence was 'humanized' by introducing human fAD mutations (*Swedish* KM670/671NL and *Beyreuther/Iberian* l716F plus additional introduction of the Arctic E693G mutation in a separate line), leads to aggressive amyloid pathology with a ~30-fold increase in the $A\beta_{42}/A\beta_{40}$ ratio.

These humanized *App* knock-in mice show early Aβ pathology including increased Aβ42 accumulation in hippocampal and cortical regions, amyloid plaques in AD-relevant brain regions as

well as microgliosis and loss of pre-synaptic synaptophysin and postsynaptic PSD95 expression [26]. Initially, cognitive phenotypes in the humanized *App* mice were only assessed using the Y-maze spontaneous exploration task and deficits emerged as late as 18 months of age (in the NL-F line). Some subsequent reports suggested a broader range of cognitive deficits including impaired spatial memory, flexible learning and reduced attention performance, associated with Aβ pathology at 18 months of age [27] and reduced locomotor activity in the absence of memory deficits [28]. Despite the apparent lag between onset of brain pathology and the behaviourally symptomatic age of these mice, their findings indicated that humanisation combined with the introduction of multiple *App* mutations produces AD-relevant pathology without APP overexpression in mice.

Here, we show that knock-in of human mutated *AβPP* (on an unaltered murine *App* background) was sufficient to produce histopathological and behavioural changes in mice. In contrast to the model generated by Saito *et al.* we knocked in a human gene construct into the mouse *Hprt* locus under CaMKIIα promoter to ensure neuron-specificity, sparing the mouse *App* gene to avoid potential changes caused by the loss of function of the endogenous gene. We report a histological and behavioural profile of singly transgenic *AβPP* mice (termed $PLB2_{APP}$) and additionally demonstrate effects of mutant *PS1* co-expression on neuronal and cognitive phenotypes in these mice.

METHODS

Animal husbandry

All animals were housed and tested in accordance with European (European Directive on the protection of animals used for scientific purposes; 2010/63/EU) and UK Home Office regulations, experiments were approved by the University Ethics Board and performed in accordance with the Animal (Scientific Procedures) Act 1986. Mice were bred and initially housed in isolators at a commercial vendor (Harlan, UK, now Envigo). After transfer to our facilities, mice were allowed to habituate for a minimum of 2 weeks; mice were group-housed in same-sex cohorts in open wire-top cages with *ad libitum* access to water and food at a circadian regime of 12 h (lights on at 7:00 A.M.) in a fully controlled environment (20 –21°C, 60–65% relative humidity). All histological and behavioural testing was performed on homozygous/hemizygous mice. Behavioural testing took place during the light period; locomotor and circadian activity in the PhenoTyper was recorded during light and dark phases over 7 days.

Generation of single mutant *APP* knock-in and *APP*/*PS1* double transgenic mice

The single transgenic $PLB2_{APP}$ mice were derived from a previously described double-transgenic mouse harbouring human, mutated *APP* and *TAU* (*APP* isoform 770 with *Swedish* and *London*

mutations; *TAU* isoform 2N4R with P301L and R406W mutations) under mouse CaMKIIα promoter cloned into the HPRT™ targeting vector [3,8] on normal endogenous $App^{+/+}$ background. Selective deletion of the *TAU* gene cassette was achieved via breeding with Flp-expressing mice. The corresponding successful excisions of the *TAU* cDNA flanked by Flipase Recognition Target (FRT) sites was confirmed (conducted by GenOway, France; for the genetic construct, see Fig. 1A). Successful insertion of the transgene in $PLB2_{APP}$ mice was determined by the presence of the 6.0 kb sized AvrII fragment of recombined *Hprt* allele in heterozygous $PLB2_{APP}$ and a lack of similar signal in the wild-type (PLB_{WT}) DNA extracts from tail biopsies via Southern blot analysis (Fig. 1B). PLB2 offspring were crossed with C57BL/6 mice for six generations before a homozygous PLB2 line was established. The CaMKIIα promoter ensures neuron- and forebrain-specific expression of the transgene; region specificity was confirmed via qPCR (Fig. 1C). RNA extraction and qPCR ($PLB2_{APP}$ mice, 6 months: n=4, 12 months, n=9) was performed as described previously [3] using MiniOpticon Real-Time PCR Detection System with iQ SYBR Green (BioRad, Hemel Hempstead, UK). We used a human *APP* specific primers (forward: 5' –ACT GGC TGA AGA AAG TGA CAA-3'; reverse: 5'ATC ACC ATC CTC ATC CTC ATC GTC CTCG-3') to detect the transgene and compare cortical and cerebellar expression. Quantification was conducted against standard serial dilutions of plasmids and copy numbers were normalised to mouse *Gapdh* (Opticon Monitor Software, BioRad, Hemel Hempstead, UK). Single transgenic $PLB2_{APP}$ mice were subsequently crossed with a previously characterised *PS1* line, containing the A246E mutation (*PS1*, B6C3H/C57BL6 background; [29]), to obtain a double transgenic $PLB2_{APP/PS1}$ line (Fig. 1D) for comparison. WT control animals were derived from the PLB_{WT} line, generated out of the breeding regime described above.

Body weights were routinely monitored before behavioural testing; data shown in Fig. 1E are from 6 months old mice (PLB_{WT}: male n=14, female n=14; $PLB2_{APP}$: male n=7, female n=8; $PLB2_{APP/PS1}$: male n=4 female n=9) and 12 months of age (PLB_{WT}: male n=10, female n=10; $PLB2_{APP}$: male n=10, female n=8; $PLB2_{APP/PS1}$: male n=11 female n=4).

Immunohistochemistry

Animals were perfused transcardially with 0.9% NaCl followed by 4% paraformaldehyde (PFA, Sigma Aldrich; in phosphate-buffered saline, PBS, pH 7.4). Brains were removed and post-fixed in PFA for <4 hrs, transferred to sodium cacodylate storage buffer (0.06M Na Cacodylate Trihydrate, pH 7.2, Sigma Aldrich) and kept at 4°C. Brain tissue was embedded in paraffin blocks and coronal sections (4.5µm) were cut on a microtome (Leica, Microsystems) from Bregma -3.0 mm to +2.5 mm in order to obtain several brain regions of interest. For quantification, stereotaxically-matched sections, based on Paxino-Watson coordinates [30], were used for quantification of

immunoreactivity (6-month groups: PLB_{WT} *n*=4, $PLB2_{APP}$ *n*=4, 12-month groups: PLB_{WT} *n*=3, $PLB2_{APP}$ *n*=4, $PLB2_{APP/PS1}$ *n*=4), and the following regions were analysed: caudal and rostral hippocampi (CA1, CA3 and DG) and cortex (see areas indicated in Fig 2C). For immunohistochemical assessment of AβPP/Aβ pathology, brain sections from PLB_{WT} and PLB2 transgenic lines were stained with 6E10 antibody (Covance, UK; dilution 1:200) using an autostainer (Leica Bond Autostaining System). Inflammation (astrogliosis) and neuronal densities were determined with manual immunofluorescence using glial fibrillary acidic protein (GFAP) (Sigma Aldrich, UK; dilution 1:400) and αNeuN antibodies (Chemicon, Millipore, UK; dilution 1:500). Primary antibodies were visualized with Bonds refined 3,3'-Diaminobenzidine (DAB) enhanced substrate system staining kit (Leica Microsystems) or appropriate AlexaFluor 488 or 594 secondary antibodies (Invitrogen; goat anti-rabbit, 1:250). Nuclei were counterstained with either haematoxylin or DAPI (Prolong Gold with DAPI, 4',6-diamidino- 2-phenylindole dihydrochloride; Sigma-Aldrich). Images were captured with a digital camera (Axiocam, Carl Zeiss) mounted on a Zeiss microscope (Axioskop 2 Plus) (x60 and x10 for 6E10 sections, x40 for GFAP sections). Staining was quantified using ImageJ as described previously [6]. Briefly, we analysed regional intracellular and extracellular 6E10 immunoreactivity (CA1, DG; parietal association cortex) by i) cell counting (DAB-positive cells normalized to total count) ii) plaque counting (per brain section), or iii) by quantifying the extracellular DAB-labelled area from binary (black and white) images (area in %) all set at identical threshold, brightness and contrast. Levels of astrogliosis are given as area stained by GFAP staining (%) and mean intensity. Brain sections used for quantification of GFAP were stained with GFAP and DAPI only to minimize potential artefacts associated with channel interference; while figures provide representative images of triple-staining (GFAP, αNeuN, DAPI) for qualitative assessment of astrocytic and neuronal co-localizations. Brain sections analysed (both hemispheres per brain region per mouse) were histologically matched and all data are expressed relative to WT. The region of interest (ROI) used for analyses was 1.2 mm x 1 mm for all brain areas (see Fig. 2C).

Behavioural analysis

Two independent cohorts of mice were used for behavioural testing at 6 and 12 months of age. Spatial reference memory (water maze) and circadian activity (PhenoTyper) were assessed in the same cohorts. Behavioural data were inspected for a possible gender effect. As gender did not affect the variables determined, data were pooled per genotype and age.

Circadian activity and habituation to a novel environment was assessed using PhenoTyper home cage system (Noldus IT, Netherlands), a video-based observation system with built-in digital

infrared lighting sources that enables continuous tracking in both dark and light periods [6,8][31]. The activity (distance moved, cm) of mice (6-month old: PLB_{WT}: male *n*=7, female *n*=8; $PLB2_{APP}$: male *n*=7, female *n*=8; $PLB2_{APP/PS1}$: male *n*=4 female *n*=7; 12-months old: PLB_{WT}: male *n*=7, female *n*=8; $PLB2_{APP}$: male *n*=9, female *n*=8; $PLB2_{APP/PS1}$: male *n*=6, female *n*=4) was recorded over 7 days at the rate of 12.5 samples/second by Ethovision software 3.1 (Noldus IT, Netherlands). Locomotor activity data were extracted in 1 hr-bin and the last 4 days were used to determine activity in fully habituated animals. Results were averaged into a) hourly-bins over 4 days (94 hrs) and b) means for 12 hrs light/dark phases. Activity during habituation (initial 3 hrs of recording) served as an indicator of exploratory behaviour in a novel environment [6]. Data were analysed using a one-phase decay fit to graphically track habituation curves of both PLB_{WT} and PLB2 animals. Initial novelty-induced exploration (Y0), activity rate constant (K; a proxy for the speed of the habituation), and plateau (stable activity level [6]) were calculated based on 10-min activity bins over 3 hrs of initial recording.

Spatial reference memory in the water maze (hereafter WM) was assessed in a 150 cm diameter and 50 cm high pool, filled with water (21 ± 1°C) with several fixed room cues visible from the pool. The procedure was identical to that described previously [3,6]. Briefly, following the visible platform test (curtains drawn, platform indicated by a flag, 4 trials of 60 seconds per mouse, randomised release sites), naïve animals (6-months old: PLB_{WT}: male *n*=7, female *n*=7; $PLB2_{APP}$: male *n*=7, female *n*=8; $PLB2_{APP/PS1}$: male *n*=4, female *n*=9; 12-months old: PLB_{WT}: male *n*=10, female *n*=8; $PLB2_{APP}$: male *n*=10, female *n*=8; $PLB2_{APP/PS1}$: male *n*=10, female *n*=4) were allocated to target platform locations (Ugo Basile, rising platforms) for 4 consecutive training days (4 trials per day, 30 min inter-trial interval, max swim time 90 sec). Swim paths, swim speed (m/sec) and thigmotaxic behaviour (distance in thigmotaxic zone, 5 cm widths) were tracked by video software (Any-Maze, Ugo Basile). On the last day of training, the platform was removed and a probe trial (60 sec) was performed 1 hr after the last training trial. Time spent in quadrants served as an indicator of spatial memory retrieval. Additional analyses were performed for *classification of search strategies* using the MATLAB (MathWorks) Strategizer approach [6]. In total, 1472 swim tracks were analysed and categorized as either: 1) random, 2) scanning, 3) chaining, 4) directed search, 5) focal search or 6) direct search using an in-house MATLAB (MathWorks) script [6] based upon algorithmic classification of these search types according to parametric definitions described before [32]. Spatial strategy data are expressed as daily means (in %) per group.

Statistical analysis

Statistical analyses were performed with Prism (V.7 GraphPad Prism) using ANOVAs (one- or two-

way Analysis of Variance) followed by Bonferroni post-tests. Behavioural data from PhenoTyper and WM tests were analysed with repeated-measure (RM) two-way ANOVA. Comparisons to chance in the WM probe test were performed with Wilcoxon signed-rank test. Non-linear regression with one-phase decay was applied for analysis of habituation to novel environment to obtain plateau, K (speed of habituation) and Y0 (starting point) values in best-fit activity curves. For WM search strategies we employed χ^2 analysis on the relative percentage composition of strategies across pairs of genotypes over 4 training days [6]. Probability of $p<0.05$ was considered reliable.

RESULTS

Breeding and general health

Breeding, litter size, overall health and attrition rates were unaffected in PLB2 mice compared to wild-type controls. Body weights of transgenic mice were not affected within each gender at either 6 or 12 months of age, independent of *PS1* status (Fig. 1 E).

Tissue analysis

Intracellular and extracellular Aβ pathology

Immunolabelling with the 6E10 antibody confirmed the subtle expression of human AβPP/Aβ in the forebrains of 12-month old $PLB2_{APP}$ and $PLB2_{APP/PS1}$ mice across several AD-relevant brain regions (Fig. 1F). Intracellular APP/Aβ histopathology was prominent in $PLB2_{APP}$ brain sections compared to age-matched WT, with a ~2.5-fold increase in Aβ-positive neurones (Fig. 1H) in the CA1 (<0.001), DG ($p<0.01$) and parietal cortex ($p<0.001$). Interestingly, $PLB2_{APP/PS1}$ mice showed similar somatic Aβ staining in cortical ($p<0.01$ compared to WT) but not hippocampal neurones, suggesting that intracellular accumulation of Aβ was differentially affected by *PS1* expression in $PLB2_{APP}$ forebrains (genotype effect across brain regions: $F_{(1,66)}=23.77$, $p<0.001$). Lack of somatic Aβ staining in the hippocampi of $PLB2_{APP/PS1}$ mice and the effect of brain region ($F_{(2,66)}=7$, $p<0.01$) further indicates that *PS1* co-expression may preferentially drive cortical Aβ pathology in $PLB2_{APP}$ mice. Extracellular Aβ accumulation was unaltered cf. WT in $PLB2_{APP}$ mice independently of brain region. Surprisingly, extracellular 6E10 immunoreactivity was somewhat lower in $PLB2_{APP/PS1}$ brain tissue (CA1: $p<0.001$, DG: $p<0.01$, cortex: $p<0.001$) compared to WT mice.

PS1 co-expression promotes Aβ plaque deposition

Amyloid plaques were sparse in $PLB2_{APP}$ mice at 12 months of age (p's>0.05 compared to controls; Fig. 1G and I). In comparison, $PLB2_{APP/PS1}$ mice displayed a higher plaque load compared to aged WT mice (Fig. 1G and I), with more frequent occurrence of both immature (<40μm in size; $p<0.05$) and diffuse plaques (>40μm; $p<0.01$). These data confirm that the presence of *PS1* decreased

extracellular soluble Aβ accumulation in favour of Aβ fibril formation in transgenic PLB2 mice.

Heightened astrogliosis but unaltered neuronal density

We further investigated the levels of brain inflammation in 6 and 12-month old $PLB2_{APP}$ mice throughout several brain regions (for localization of brain regions selected, see Fig. 2C) relevant to cognition using an astrocyte-specific GFAP antibody (Fig. 2, GFAP visualised in green). At 6 months (Fig. 2A-B) $PLB2_{APP}$ mice showed increased astrogliosis (area; in %) within the neuronal layer of DG and CA1 compared to WT controls ($p<0.05$ and $p<0.001$, respectively; Fig. 2C-D) while CA3 and entorhinal cortex (EC) were unaltered at this age. GFAP staining intensity was also increased in the hippocampal CA1 and DG regions in $PLB2_{APP}$ mice compared to controls ($p>0.01$; Fig. 2E). Double-transgenic $PLB2_{APP/PS1}$ mice were not assessed histologically at 6 months due to lack of tissue for this age group. At 12-months of age, hippocampal inflammation was still evident in $PLB2_{APP}$ mice (Fig. 3A), with a ~2-fold increase in the total area covered by astrocytes ($p<0.01$, GFAP visualised in red) compared to controls, and the cortical region analysed remained unaffected (Fig. 3B). In contrast, $PLB2_{APP/PS1}$ mice showed increased cortical ($p<0.01$), but not hippocampal astrogliosis ($p=0.09$). For the older cohorts, GFAP intensity was also increased in hippocampal DG ($p<0.05$) and cortical region in $PLB2_{APP}$ mice compared to controls ($p<0.001$, Fig. 3C), while $PLB2_{APP/PS1}$ mice had significantly increased GFAP intensity in the cortex only ($p<0.01$).

In order to determine the effects of transgene(s) on neuronal density / cell loss in PLB2 mice we quantified neuronal bodies using the αNeuN antibody. The number of neurons (expressed as % of total cell count; Fig. 3D) did not differ between transgenic lines and WT controls, independently of ROI used ($F<1$, $p>0.05$; Fig. 3E), suggesting no frank cell loss in these mice at one year of age.

Behavioural alterations

Delayed habituation to a novel environment in $PLB2_{APP}$ mice

Gross locomotor activity during the first 3 hrs of the recording did not differ between transgenic lines and WT mice at 6 months of age. However, $PLB2_{APP}$ animals displayed slower habituation (altered activity rate constant, K) compared to age-matched controls ($p<0.01$; Fig. 4A), suggesting a possible delay in the formation of a spatial map for the novel environment [6,33]. This phenotype was also detected, though to a lesser extent, in 6-month old $PLB2_{APP/PS1}$ mice (K: $p<0.05$ compared to WT). Interestingly, at 12 months $PLB2_{APP}$ mice continued to display delayed habituation relative to WT (altered K, $p<0.05$; Fig. 4B) while age-matched $PLB2_{APP/PS1}$ animals did not. Slower habituation did not affect the plateau in PLB2 mice at either age point. The delayed habituation to novel environment in $PLB2_{APP}$ mice was exacerbated from 6 to 12 months, with a reduced activity rate constant (K, $p<0.05$) and lower initial activity (Y0; $p<0.001$) in the older age group. WT mice

showed similar trends for age-induced deterioration of habituation (K, $p<0.05$, Y0, $p=0.06$, plateau, $p=0.056$), but no effect of age was detected in $PLB2_{APP/PS1}$ animals ($p's>0.05$).

Global reductions in locomotor activity in PLB2 mice: Age-dependent changes in $PLB2_{APP}$ but not $PLB2_{APP/PS1}$ mice

Overall locomotor activity in habituated animals was unchanged in 6-month old $PLB2_{APP}$ mice compared to controls ($p>0.05$), but reduced in age-matched double transgenic $PLB2_{APP/PS1}$ mice ($F_{(1,552)}=5.5$, $p<0.05$; Fig. 4C). Home-cage activity differed between the two transgenic lines at this age ($F_{(1,552)}=4.8$, $p<0.05$), suggesting an early emergence of a hypoactive phenotype in the *PS1* co-expressing mice.

By 12 months of age, $PLB2_{APP}$ mice showed a robust global reduction in locomotor activity compared to aged WT's ($F_{(1,690)}=21.25$, $p<0.001$; Fig. 4D). Here again, an ageing effect was observed only in single transgenic mice ($F(1,690)=26.3$, $p<0.001$). No age effect was apparent in the control group or $PLB2_{APP/PS1}$ animals, which continued to exhibit decreased activity at this age group ($F(1,529)=7.9$, $p<0.01$; Fig. 4D). Data pooled for light/dark periods (see Fig. 4E) confirmed global reductions in locomotion in $PLB2_{APP/PS1}$ from 6 months (light, $p<0.01$; and dark, $p<0.05$) and from 12 months of age in $PLB2_{APP}$ mice (light, $p<0.001$; dark, $p<0.001$).

Impaired spatial reference memory and strategy adaptation in PLB2 animals

We used the standard WM task to investigate whether forebrain-specific expression of mutant *APP* in mice was sufficient to alter spatial learning and retrieval in mice, and to evaluate effects of co-expression of *PS1* on cognitive profile of $PLB2_{APP}$ mice. Visual ability test (prior to hidden platform training) demonstrated that $PLB2_{APP/PS1}$ mice covered longer distances to find the platform (PF) during the first 2 trials ($p<0.01$ and $p<0.05$ compared to controls, Fig. 5A and C). This was likely due to an anxious response to the test as indicated by increased thigmotaxic behaviour compared to WT controls (see Fig. 5G). However, swim paths to visible PF were unaltered in $PLB2_{APP/PS1}$ animals during trials 3 and 4, demonstrating intact visual abilities in these mice (individual trial data, Fig. 5A and C). $PLB2_{APP}$ mice located the visible PF comparable to age-matched controls, independent of age ($p's >0.05$).

During acquisition days (hidden platform training days 1-4), a robust deficit was detected in 6-month old $PLB2_{APP}$ ($F_{(1,81)}=18.42$, $p<0.001$, Fig. 5A and E) and in $PLB2_{APP/PS1}$ mice compared to age-matched WT ($F_{(1,75)}=4.3$, $p<0.05$, Fig. 5A and E). Both transgenic lines continued to exhibit a significant impairment in spatial learning at 12 months of age ($PLB2_{APP}$: $F_{(1,102)}=9.1$, $p<0.01$; $PLB2_{APP/PS1}$: $F_{(1,90)}=17.8$, $p<0.001$; Fig. 5C and F). No effects of genotype were found between the two transgenic groups for the older cohorts ($F's<1$, $p's>0.05$).

Time in thigmotaxic zone was increased in $PLB2_{APP}$ mice compared to controls at 6 months ($F_{(1,81)}$=15.6, p<0.001; especially during day 1 of training, p<0.001; Fig. 5G). At 12 months, the thigmotaxic behaviour of $PLB2_{APP}$ animals was unaltered (F<1, p>0.05; Fig. 5I). Interestingly, $PLB2_{APP/PS1}$ mice had unaltered thigmotaxic behaviour during training days independent of age (Fs'<1, p's>0.05; Fig. 5G and I). Swim speed varied between groups, with 6-month old $PLB2_{APP}$ showing increased velocity compared to $PLB2_{APP/PS1}$ ($F_{(1,78)}$=5.1, p<0.05; Fig. 5H) but not compared to WT (F<1, p>0.05), and at 12 months $PLB2_{APP/PS1}$ animals showed increased swimming velocity compared to both WT ($F_{(1,90)}$=17.6, p<0.001) and $PLB2_{APP}$ mice ($F_{(1,90)}$=9.1, p<0.01; Fig. 5J). The swim speed also declined with age in WT and $PLB2_{APP}$ mice (age effects, WT: $F_{(1,90)}$=18.4, p<0.001; $PLB2_{APP}$: $F_{(1,93)}$=24.2, p<0.0001) but not in $PLB2_{APP/PS1}$ animals (F<1, p>0.05).

To test memory retrieval post-acquisition we employed a probe trial where the platform was removed and time in target quadrant was measured for 60 sec. All groups demonstrated intact recall for target location ($p \leq 0.05$ cf. level of chance, 15sec) independently of genotype or age. However, 6-month old $PLB2_{APP}$ mice spent significantly less time in the target quadrant compared to age-matched controls (t=1.8, df=25, p<0.05; Fig. 5B); $PLB2_{APP/PS1}$ mice did not show similar trends. Within-genotype comparisons indicated that age did not affect memory in either of the lines (p's>0.05).

We further employed the strategy analysis to determine whether the compromised path length to target during learning was indeed associated with poor cognitive (non-spatial) strategies (Fig. 6A). Strategy profiling revealed pronounced genotype differences between transgenic groups and WT controls both at 6 (Fig. 6B-D) and 12 months of age (Fig. 6E-G). Distribution of strategies (daily averages, %) per group and per training days were analysed with Chi-square (for a summary data table, see Fig. 6H). Six-month old $PLB2_{APP}$ employed significantly less spatial navigation (-20 to -35% less directed, focal or direct searches) compared to controls throughout all training days (1-4), and other non-spatial search strategies (i.e. chaining and scanning) were more frequent in these mice. Similarly, age-matched $PLB2_{APP/PS1}$ mice showed altered strategy distribution, yet this was evident only from day 2 of training. Interestingly, spatial search scores were significantly improved in $PLB2_{APP/PS1}$ animals (+25% spatial) compared to single-transgenic $PLB2_{APP}$ mice at 6-months during day 2 of training ($\chi 2$=47, p<0.001; Fig. 6. C-D). At 12 months strategies did not differ between the two transgenic lines, and only $PLB2_{APP/PS1}$ mice showed significantly reduced spatial navigation during days 3 and 4 only (-20% compared to aged WT controls).

DISCUSSION

In light of the rapidly growing worldwide prevalence of AD, the most common cause of dementia, the search for a disease-modifying treatment remains one of the biggest challenges in modern medicine. Although early-onset fAD accounts for <1% of all AD cases, the respective mutations are continuing to guide experimental modelling of AD in preclinical studies. Thus far, more than 20 mutations in the *AβPP* [34] and >200 mutations in the *PS1* or *PS2* genes [35] were identified as determinants of autosomal dominant fAD, corroborating the relevance of Aβ pathology in AD pathogenesis. Clinically, AD is characterized by memory deficits followed by a decline in other cognitive and executive functions [36]. Accumulation of soluble Aβ as well as phospho-tau and pathological tau oligomers emerge before overt cognitive symptoms and track disease progression in human AD [37,38]. Other sources suggest that Aβ pathology emerges at least two decades before cortical tau pathology and the onset of medical symptoms [39,40] when postmitotic neurons start to degenerate. Over the last decades, >400 drug candidates failed to reach the clinic [41,42]; this large-scale failure has been attributed to inappropriate mouse models in preclinical studies, the timing for therapeutic interventions, and the lack of appropriate biomarkers for early diagnosis, to mention but a few. The development of better animal models that accurately mimic early pathogenic events as observed in human AD is now considered vital for advances in both diagnostic and therapeutic strategies.

Based on fAD gene mutations, various transgenic mouse models have been generated for preclinical studies. The vast majority of these models rely on transgenic overexpression of human, mutated *AβPP*, alone or in combination with *TAU* and *PS1*, giving rise to elevated levels of Aβ to reiterate amyloidosis. However, in addition to amyloidogenic pathology, these mice express high levels of the full-length AβPP, therefore over-burdening the proteostasis apparatus with AβPP and its multiple cleavage products. Given their complex roles, a misbalance in AβPP handling may *per se* lead to a variety of cellular responses in addition to the gain of toxic function of Aβ fragments, hence resulting in a number of effects not genuinely related to Aβ pathology. The first generation AD mice also relied on random transgene integration in unknown loci, likely causing artefacts related to perturbation of the host genome (transgenic mutagenesis), random topography of protein expression, uncontrolled developmental abnormalities [2,43], alongside high translational demand and cellular stress unrelated to the innate transgene function [44,45]. The genetic murine background was also previously shown to modify amyloid pathology [46] making it difficult to directly compare the existing animal models of AD with each other.

To overcome these drawbacks, recent efforts have been made to develop mouse models that produce Aβ in a controlled manner without overexpressing AβPP. We have generated a series of novel mouse lines (collectively termed PLB) on the same genetic background using homologous recombination knock-in strategy to introduce a single copy of a transgene into the *Hprt* locus under a neuron-specific CaMKIIα promoter. Similarly to the previously reported $PLB1_{Triple}$, $PLB2_{Tau}$ and $PLB4_{BACE1}$ mice, the $PLB2_{APP}$ mice described here demonstrate mild forebrain-specific expression of the human transgene to allow for investigation of histopathological and behavioural alterations specific to the mutations within the *AβPP* transgene. Our histological assessment demonstrates that the expression of human *AβPP* carrying *Swedish* and *London* mutations was sufficient to produce intracellular and subtle extracellular Aβ build-up primarily affecting the hippocampal regions. The amyloidogenic changes were accompanied by heightened astrogliosis as shown by GFAP staining at 6 and 12 months of age in $PLB2_{APP}$ mice. Although further studies are needed to confirm the exact nature of species detected with the $PLB2_{APP}$ hippocampi, it is likely that the 6E10-immunoreactive Aβ comprises soluble oligomers similar to those observed in $PLB1_{Triple}$ mice carrying the same *AβPP* transgene [3,4,6]. Notably, these histopathological changes coincided with delayed habituation to novel environment and decreased locomotor activity, preceding spatial learning impairments in the water maze at 12 months of age.

Our findings from the $PLB2_{APP}$ model suggest that cognitive deficits can be induced in mice by a single-copy gene knock-in of human, mutant *AβPP* without overexpression or significant plaque formation. Moreover, the CaMKIIα promoter utilised here mimics the neuronal expression pattern of human AβPP pathology [47] by limiting expression to forebrain regions and by reducing the risk of potential artefacts associated with temporal and spatial distribution of the transgene. The likely cause of behavioural deficits in these mice is human Aβ fragments accumulating preferentially within hippocampal neurons, followed by a similar regional activation of astrocytes. Of note, the presence of endogenous murine *App* gene in $PLB2_{APP}$ mice may have affected their phenotype, and it is at present unclear if this is an advantage or disadvantage. Although novel knock-in technology to introduce *App* mutations as utilized by the Saito group may appear to yield higher face validity for the human condition due to specific 'humanized' AβPP -derived products, it is unclear how the loss of function of endogenous APP protein has affected mouse brain physiology and cognition. Importantly, the humanized *App* may also have a distinct biochemical profile as the *App* gene, except for parts of intron 15–17, is still murine. For example, the KPI domain (Kunitz-type protease inhibitor domain in the extracellular region) containing variants of APP are expressed in human but not mouse AβPP [26]. It is therefore not entirely clear whether metabolism and cleavage of this form of AβPP by murine secretases is a reflection of human and/or murine pathways. The

role of the murine *App* promoter is an obvious advantage of the humanised knock-in mouse, though no comparative study exists addressing the differences between mouse and human spatio-temporal expression of APP isoforms and *App*/*APP* gene promoters.

Similarly to $PLB2_{APP}$ mice and other AD models, *App* knock-in mice contain a combination of two or three independent fAD mutations, which do not occur together in human fAD cases and may lead to an unusual Aβ conformation [48]. This may drive fibrillation and plaque formation, but not necessarily lead to raised levels of toxic, soluble species, as indicated by the disconnect between amyloid pathology and late behavioural phenotypes in the humanised *App* model [49], though a comparison with wild-type controls was missing from this latest study. Altogether, second generation *AβPP* knock-in mice have improved our understanding of Aβ pathology but fall short of fully explaining its role in cognitive dysfunction in human AD.

Here, we have additionally crossed the $PLB2_{APP}$ mice to the *PS1* mutant carrying the A246E mutation to further facilitate AβPP cleavage. In the double transgenic $PLB2_{APP/PS1}$ mouse Aβ pathology shifted from hippocampal to cortical localization compared to the single transgenic mice. Similarly, patterns of glia emergence and activation followed the temporal patterns of Aβ accumulation, i.e. $PLB2_{APP}$ mice showed primarily hippocampal histopathology, while double transgenic mice co-expressing *PS1* presented with amyloid and GFAP pathology in cortical areas where plaque deposition was also more frequent. This is in agreement with a recent report that suggested co-expression of $PS1^{M233T/L235P}$ via knock-in in $APP^{Swe/Lon}$ mice induced substantial region-specific Aβ accumulation preceding neuronal and synaptic loss [50].

However, the contribution of this pathology to cognitive changes *in vivo* has not been described. Behaviourally, $PLB2_{APP}$ mice displayed delayed habituation to a novel environment during the initial 3 hrs of familiarization [6,33]. $PLB2_{APP/PS1}$ mice demonstrated mild changes in habituation rates at 6 months and a somewhat preserved phenotype at the age of 12 months. Locomotor activity in habituated mice was reduced in the double $PLB2_{APP/PS1}$ mice at 6 months to a larger extend compared to $PLB2_{APP}$ mice, which displayed similar reductions at 12 months only. These data suggest that co-expression of *PS1* may have induced an earlier reduction (potentially to floor level) in locomotor activity and hence occluded the age-dependent exacerbation of the phenotype seen in $PLB2_{APP}$ mice. The hippocampus-dependent spatial learning in the WM was affected in single $PLB2_{APP}$ mice at 6 months particularly during the initial days of training, again suggesting impaired navigation in novel environment. Interestingly, in contrast to single transgenic mice, $PLB2_{APP/PS1}$ managed to locate the target during the initial training and only the following acquisition days were affected compared to controls. At 12 months, both mouse lines demonstrated impaired spatial

learning compared to WT mice. These differences were associated with decreased use of spatial strategies in $PLB2_{APP}$ and $PLB2_{APP/PS1}$ mice in a day- and genotype-dependent manner. Thus, co-expression of *PS1* in a human mutated *AβPP* transgenic exacerbates activity-related phenotypes but not cognitive processes dependent on hippocampal function.

Altogether, our findings demonstrate that knock-in of single copy human fAD mutant *AβPP* gene in neurons is sufficient to cause subtle hippocampal histopathology and age-dependent behavioural changes in mice, akin to early changes in fAD individuals, such as impaired spatial learning, reduced activity and circadian rhythmicity. Despite potential drawbacks as no full-blown plaque pathology, NFTs and overt neuronal loss developed in these mice, they offer advantages as preclinical models for the identification of early physiological biomarkers and to study the response of astrocytes upon amyloid stress.

Author contributions

KP wrote the manuscript with input from BP. KP carried out the main experimental work. BC performed the strategy analysis of water maze tracks, JMY contributed to histological analyses and SS performed qPCR experiments. BP and GR designed the transgenic mice and the study endpoints. All authors approved the final version of the manuscript.

Funding sources

KP was funded by a donation from Roemex Ltd (Mr. R. Simcox) to BP and GR. The project was in part supported by the Alzheimer's Research UK (ARUK) Scotland network and by an Alzheimer's Society project grant (AS-PG-14-039) to BP and GR.

Conflict of interest statement

The authors declare that there is no conflict of interest associated with this manuscript.

Figure legends

Figure 1. The *APP* transgene construct in $PLB2_{APP}$ mouse models, *PS1* cross-breeding and effects of both genotypes on amyloid histopathology in aged mice. **(A)** Schematic representation of the knock-in strategy of $PLB2_{APP}$ line post Flp-mediated excision of the FRT-flanked region (for details, see text). **(B)** Southern blot analysis of the $PLB2_{APP}$ F1 generation. The genomic DNA of the 12 tested mice was compared with wild-type DNA (129ES, BL6). Digested DNA samples were blotted on a nylon membrane and hybridised with the 5' probe to validate the zygocity of the *Hprt*-CaMKIIα-*APP*-allele in these animals. $PLB2_{APP}$ (Hprt-CaMKII-APP) genotype: 19573, 19706; $PLB2_{APP/TAU}$ (Hprt-CaMKII-APP-TAU) genotype: 19749, 19753, 19575, 19704, 19705. **(C)** Quantitative *APP* mRNA expression $PLB2_{APP}$ mice and PLB_{WT} controls. **(D)** Genetic design of the pre-existing *PS1* mouse line used for the generation of generation of $PLB2_{APP/PS1}$ mice. **(E)** Body weights of $PLB2_{APP}$ and $PLB2_{APP/PS1}$ mice. (**F**) AβPP and Aβ histopathology in $PLB2_{APP}$ and $PLB2_{APP/PS1}$ mice at 12 months of age using anti-human 6E10 antibody across hippocampal (CA1 and DG) and cortical regions. Arrows indicate enhanced extracellular staining in CA1 region of $PLB2_{APP}$ mice and lack of similar deposition in $PLB2_{APP/PS1}$ mice; as well as increased intracellular staining (AβPP positive neurons) in the cortex of $PLB2_{APP/PS1}$ compared to the cortices of $PLB2_{APP}$ mice. Scale bar indicates 100µm (magnification x63). (**G**) High-power representative images of amyloid plaque deposition in both transgenic lines and WT controls. Scale bar indicates 400µm (magnification x10). (**H**) Quantification of intra- and extra-cellular 6E10-immunoreactivity. (**I**) An average number of Aβ plaques (divided by size) in whole brain coronal section of PLB2 and WT animals. Abbreviations: *CA1* Cornu Ammonis 1, *Cere* Cerebellum, *CTX* cortex (parietal), *DG* Dentate Gyrus. Data were normalized to controls and represent mean + SEM. Significances: * $p<0.05$, ** $p<0.01$, *** $p<0.001$.

Figure 2. Regional expression and quantification of GFAP-labelled astrocytes co-localizing neuronal bodies across several AD-relevant brain regions in 6-month $PLB2_{APP}$ old mice. (**A)** Representative images of 6-month old WT (left panel) and **(B)** 6-month old $PLB2_{APP}$ hippocampal (DG, CA1, CA3) and entorhinal cortex (EC). Note, astrocyte infiltration was evident within neuronal layers as well as in neuronal processes in $PLB2_{APP}$ hippocampi as indicated by the arrows in panel B. the arrows **(C)** Quantification of the total area covered by GFAP-labelled astrocytes and **(D)** intensity of the stain. Green: astrocytes (GFAP), red: neuronal bodies (αNeuN antibody), blue: nuclei (DAPI). Abbreviations: *DG* Dentate Gyrus, *CA1/*3 Cornu Ammonis 1/3, *EC* Entorhinal Cortex, *m* months. The scale bar indicates 50µm (magnification x40). ***: $p<0.001$. Data represent mean + SEM.

Figure 3. Astrogliosis and neuronal densities in brain tissue from 12-month old PLB2 and WT mice. (**A)** Representative immunofluorescent images of the polymorph layer of the DG and cortex (GFAP: red; cell bodies: blue). (**B)** Quantification of astroglyosis (total area covered in %) and mean GFAP intensity **(C)** in 12-month old WT, $PLB2_{APP}$ and $PLB2_{APP/PS1}$ mice. (**D)** Representative images of neurones (αNeuN: red, cell bodies: blue) in 12-month old mice. (**E)** Quantification of neuronal densities in transgenic PLB2 mice and WT controls. Abbreviations: *DG* Dentate Gyrus, *CTX* Cortex, *m* months. Scale bars indicate 50µm (magnification x40). Asterisks: * $p<0.05$, ** $p<0.01$, *** $p<0.001$. Data were normalized relative to controls and represent mean + SEM.

Figure 4. Habituation to a novel environment, locomotor and circadian activity in $PLB2_{APP}$ and $PLB2_{APP/PS1}$ mice. (**A-B)** Nonlinear regression analyses of activity (distance moved, cm) of PLB_{WT} controls, $PLB2_{APP}$ and $PLB2_{APP/PS1}$ mice during habituation (3 hrs) in the PhenoTyper home cage at 6 and 12 months of age. **(C-D)** Global ultradian activity (96-hr in hourly-bins averaged over 24hrs). (**E)** Mean distance moved (+SEM) pooled for light and dark phases (12 hrs each). Significances: * $p<0.05$, ** $p<0.01$, *** $p<0.001$. Data represent mean ± or + SEM.

Figure 5. Spatial reference memory in $PLB2_{APP}$, $PLB2_{APP/PS1}$ and PLB_{WT} mice at 6 and 12 months of age in the water maze paradigm. (**A)** and **(C)** Mean path lengths to platform for each day of training in $PLB2_{APP}$ and $PLB2_{APP/PS1}$ mice at 6 and 12 months of age compared to age-matched WT controls. (**B)** and (**D)** Probe trial (memory recall test) 1hr post training on day 4. (**E**–**F)** Representative swim paths for acquisition days (A1-A4 with hidden platform) and probe trial (P). **G-J**: Thigmotaxic behaviour and swim speed of 6-month old and 12-month old $PLB2_{APP}$ mice and $PLB2_{APP/PS1}$ mice cf. PLB_{WT} controls. Abbreviations: *Vis PF* visible platform. Asterisks: * $p<0.01$, ** $p<0.01$, *** $p<0.001$. Data represent mean ± SEM or + SEM.

Figure 6. Analyses of search strategies employed to locate the hidden platform in the water maze in 6- and 12-month old $PLB2_{APP}$, $PLB2_{APP/PS1}$ and PLB_{WT} (WT) mice. **(A)** Classification of search strategies, representative sample traces and colour codes of identified categories commonly used by rodents in the water maze test. Mean relative occurrence of each strategy represented for the four spatial acquisition days for 6-month old PLB_{WT} (**B**), $PLB2_{APP}$ **(C)**, $PLB2_{APP/PS1}$ (**D**) and 12-month old PLB_{WT} (**E**), $PLB2_{APP}$ (**F**) and $PLB2_{APP/PS1}$ mice **(G)**. (**H**) The table represents reliable genotype differences based on contingency plots between age-matched groups, with α set to 5%. Grey shaded boxes highlight training days with robustly different strategy compositions.

References

[1] Selkoe DJ, Hardy J (2016) The amyloid hypothesis of Alzheimer's disease at 25 years. *EMBO Mol Med* **8**, 595-608.

[2] Sasaguri H, Nilsson P, Hashimoto S, Nagata K, Saito T, De Strooper B, Hardy J, Vassar R, Winblad B, Saido TC (2017) APP mouse models for Alzheimer's disease preclinical studies. *EMBO J* **36**, 2473-2487.

[3] Platt B, Drever B, Koss D, Stoppelkamp S, Jyoti A, Plano A, Utan A, Merrick G, Ryan D, Melis V, Wan H, Mingarelli M, Porcu E, Scrocchi L, Welch A, Riedel G (2011) Abnormal cognition, sleep, EEG and brain metabolism in a novel knock-in Alzheimer mouse, PLB1. *PLoS ONE* **6**.

[4] Koss DJ, Drever BD, Stoppelkamp S, Riedel G, Platt B (2013) Age-dependent changes in hippocampal synaptic transmission and plasticity in the PLB1Triple Alzheimer mouse. *Cell Mol Life Sci* **70**, 2585-2601.

[5] Ryan D, Koss D, Porcu E, Woodcock H, Robinson L, Platt B, Riedel G (2013) Spatial learning impairments in PLB1Triple knock-in Alzheimer mice are task-specific and age-dependent. *Cell Mol Life Sci* **70**, 2603-2619.

[6] Plucinska K, Crouch B, Koss D, Robinson L, Siebrecht M, Riedel G, Platt B (2014) Knock-in of human BACE1 cleaves murine APP and reiterates Alzheimer-like phenotypes. *J Neurosci* **34**, 10710-10728.

[7] Plucinska K, Dekeryte R, Koss D, Shearer K, Mody N, Whitfield PD, Doherty MK, Mingarelli M, Welch A, Riedel G, Delibegovic M, Platt B (2016) Neuronal human BACE1 knockin induces systemic diabetes in mice. *Diabetologia* **59**, 1513-1523.

[8] Koss DJ, Robinson L, Drever BD, Plucinska K, Stoppelkamp S, Veselcic P, Riedel G, Platt B (2016) Mutant Tau knock-in mice display frontotemporal dementia relevant behaviour and histopathology. *Neurobiol Dis* **91**, 105-123.

[9] Masliah E, Sisk A, Mallory M, Mucke L, Schenk D, Games D (1996) Comparison of neurodegenerative pathology in transgenic mice overexpressing V717F/β-amyloid precursor protein and Alzheimer's disease. *J Neurosci* **16**, 5795-5811.

[10] Chen KS, Masliah E, Grajeda H, Guido T, Huang J, Khan K, Motter R, Soriano F, Games D (1998) Neurodegenerative Alzheimer-like pathology in PDAPP 717V→F transgenic mice. *Prog Brain Res* **117**, 327-334.

[11] Hsiao K, Chapman P, Nilsen S, Eckman C, Harigaya Y, Younkin S, Yang F, Cole G (1996) Correlative memory deficits, Aß elevation, and amyloid plaques in transgenic mice. *Science* **274**, 99-102.

[12] Sturchler-Pierrat C, Abramowski D, Duke M, Wiederhold K-, Mistl C, Rothacher S, Ledermann B, Bürki K, Frey P, Paganetti PA, Waridel C, Calhoun ME, Jucker M, Probst A, Staufenbiel M, Sommer B (1997) Two amyloid precursor protein transgenic mouse models with Alzheimer disease-like pathology. *Proc Natl Acad Sci U S A* **94**, 13287-13292.

[13] Mucke L, Masliah E, Yu G-, Mallory M, Rockenstein EM, Tatsuno G, Hu K, Kholodenko D, Johnson-Wood K, McConlogue L (2000) High-level neuronal expression of Aß(1-42) in wild-type

human amyloid protein precursor transgenic mice: Synaptotoxicity without plaque formation. *J Neurosci* **20**, 4050-4058.

[14] Chishti MA, Yang D-, Janus C, Phinney AL, Horne P, Pearson J, Strome R, Zuker N, Loukides J, French J, Turner S, Lozza G, Grilli M, Kunicki S, Morissette C, Paquette J, Gervais F, Bergeron C, Fraser PE, Carlson GA, St. George-Hyslop P, Westawaya D (2001) Early-onset Amyloid Deposition and Cognitive Deficits in Transgenic Mice Expressing a Double Mutant Form of Amyloid Precursor Protein 695. *J Biol Chem* **276**, 21562-21570.

[15] Citron M, Oltersdorf T, Haass C, McConlogue L, Hung AY, Seubert P, Vigo-Pelfrey C, Lieberburg I, Selkoe DJ (1992) Mutation of the ß-amyloid precursor protein in familial Alzheimer's disease increases ß-protein production. *Nature* **360**, 672-674.

[16] Theuns J, Brouwers N, Engelborghs S, Sleegers K, Bogaerts V, Corsmit E, De Pooter T, Van Duijn CM, De Deyn PP, Van Broeckhoven C (2006) Promoter mutations that increase amyloid precursor-protein expression are associated with Alzheimer disease. *Am J Hum Genet* **78**, 936-946.

[17] Theuns J, Marjaux E, Vandenbulcke M, Van Laere K, Kumar-Singh S, Bormans G, Brouwers N, Van Den Broeck M, Vennekens K, Corsmit E, Cruts M, De Strooper B, Van Broeckhoven C, Vandenberghe R (2006) Alzheimer dementia caused by a novel mutation located in the APP C-terminal intracytosolic fragment. *Hum Mutat* **27**, 888-896.

[18] Herl L, Thomas AV, Lill CM, Banks M, Deng A, Jones PB, Spoelgen R, Hyman BT, Berezovska O (2009) Mutations in amyloid precursor protein affect its interactions with presenilin/γ-secretase. *Mol Cell Neurosci* **41**, 166-174.

[19] Karch CM, Cruchaga C, Goate AM (2014) Alzheimer's disease genetics: From the bench to the clinic. *Neuron* **83**, 11-26.

[20] De Strooper B, Saftig P, Craessaerts K, Vanderstichele H, Guhde G, Annaert W, Von Figura K, Van Leuven F (1998) Deficiency of presenilin-1 inhibits the normal cleavage of amyloid precursor protein. *Nature* **391**, 387-390.

[21] Zhang Z, Hartmann H, Do VM, Abramowski D, Sturchler-Pierrat C, Staufenbiel M, Sommer B, Van De Wetering M, Clevers H, Saftig P, De Strooper B, He X, Yankner BA (1998) Destabilization of ß-catenin by mutations in presenilin-1 potentiates neuronal apoptosis. *Nature* **395**, 698-702.

[22] Borchelt DR, Thinakaran G, Eckman CB, Lee MK, Davenport F, Ratovitsky T, Prada C-, Kim G, Seekins S, Yager D, Slunt HH, Wang R, Seeger M, Levey AI, Gandy SE, Copeland NG, Jenkins NA, Price DL, Younkin SG, Sisodia SS (1996) Familial Alzheimer's disease-linked presenilin I variants elevate aß1- 42/1-40 ratio in vitro and in vivo. *Neuron* **17**, 1005-1013.

[23] Holcomb L, Gordon MN, Mcgowan E, Yu X, Benkovic S, Jantzen P, Wright K, Saad I, Mueller R, Morgan D, Sanders S, Zehr C, O'Campo K, Hardy J, Prada C-, Eckman C, Younkin S, Hsiao K, Duff K (1998) Accelerated Alzheimer-type phenotype in transgenic mice carrying both mutant amyloid precursor protein and presenilin 1 transgenes. *Nat Med* **4**, 97-100.

[24] Borchelt DR, Ratovitski T, Van Lare J, Lee MK, Gonzales V, Jenkins NA, Copeland NG, Price DL, Sisodia SS (1997) Accelerated amyloid deposition in the brains of transgenic mice coexpressing mutant presenilin 1 and amyloid precursor proteins. *Neuron* **19**, 939-945.

[25] Casas C, Sergeant N, Itier J-, Blanchard V, Wirths O, Van Der Kolk N, Vingtdeux V, Van De Steeg E, Ret G, Canton T, Drobecq H, Clark A, Bonici B, Delacourte A, Benavides J, Schmitz C, Tremp G, Bayer TA, Benoit P, Pradier L (2004) Massive CA1/2 neuronal loss with intraneuronal and N-terminal truncated Aß42accumulation in a novel Alzheimer transgenic model. *Am J Pathol* **165**, 1289-1300.

[26] Saito T, Matsuba Y, Mihira N, Takano J, Nilsson P, Itohara S, Iwata N, Saido TC (2014) Single App knock-in mouse models of Alzheimer's disease. *Nat Neurosci* **17**, 661-663.

[27] Masuda A, Kobayashi Y, Kogo N, Saito T, Saido TC, Itohara S (2016) Cognitive deficits in single App knock-in mouse models. *Neurobiol Learn Mem* **135**, 73-82.

[28] Whyte LS, Hemsley KM, Lau AA, Hassiotis S, Saito T, Saido TC, Hopwood JJ, Sargeant TJ (2018) Reduction in open field activity in the absence of memory deficits in the AppNL-G-Fknock-in mouse model of Alzheimer's disease. *Behav Brain Res* **336**, 177-181.

[29] Jyoti A, Plano A, Riedel G, Platt B (2010) EEG, activity, and sleep architecture in a transgenic AßPP swe/PSEN1A246E Alzheimer's disease mouse. *J Alzheimer's Dis* **22**, 873-887.

[30] Franklin K, Paxinos G (2008) The Mouse Brain in Stereotaxic Coordinates, Compact, 3rd Edition.

[31] Robinson L, Spruijt B, Riedel G (2017) Between and within laboratory reliability of mouse behaviour recorded in home-cage and open-field. *J Neurosci Methods* .

[32] Garthe A, Behr J, Kempermann G (2009) Adult-generated hippocampal neurons allow the flexible use of spatially precise learning strategies. *PLoS ONE* **4**.

[33] Robinson L, Plano A, Cobb S, Riedel G (2013) Long-term home cage activity scans reveal lowered exploratory behaviour in symptomatic female Rett mice. *Behav Brain Res* **250**, 148-156.

[34] Hunter S, Brayne C (2018) Understanding the roles of mutations in the amyloid precursor protein in Alzheimer disease. *Mol Psychiatry* **23**, 81-93.

[35] Lanoiselée H-, Nicolas G, Wallon D, Rovelet-Lecrux A, Lacour M, Rousseau S, Richard A-, Pasquier F, Rollin-Sillaire A, Martinaud O, Quillard-Muraine M, de la Sayette V, Boutoleau-Bretonniere C, Etcharry-Bouyx F, Chauviré V, Sarazin M, le Ber I, Epelbaum S, Jonveaux T, Rouaud O, Ceccaldi M, Félician O, Godefroy O, Formaglio M, Croisile B, Auriacombe S, Chamard L, Vincent J-, Sauvée M, Marelli-Tosi C, Gabelle A, Ozsancak C, Pariente J, Paquet C, Hannequin D, Campion D (2017) APP, PSEN1, and PSEN2 mutations in early-onset Alzheimer disease: A genetic screening study of familial and sporadic cases. *PLoS Med* **14**.

[36] Winblad B, Amouyel P, Andrieu S, Ballard C, Brayne C, Brodaty H, Cedazo-Minguez A, Dubois B, Edvardsson D, Feldman H, Fratiglioni L, Frisoni GB, Gauthier S, Georges J, Graff C, Iqbal K, Jessen F, Johansson G, Jönsson L, Kivipelto M, Knapp M, Mangialasche F, Melis R, Nordberg A, Rikkert MO, Qiu C, Sakmar TP, Scheltens P, Schneider LS, Sperling R, Tjernberg LO, Waldemar G, Wimo A, Zetterberg H (2016) Defeating Alzheimer's disease and other dementias: A priority for European science and society. *Lancet Neurol* **15**, 455-532.

[37] Koss DJ, Jones G, Cranston A, Gardner H, Kanaan NM, Platt B (2016) Soluble pre-fibrillar tau and ß-amyloid species emerge in early human Alzheimer’s disease and track disease progression and cognitive decline. *Acta Neuropathol* **132**, 875-895.

[38] Hyman BT, Phelps CH, Beach TG, Bigio EH, Cairns NJ, Carrillo MC, Dickson DW, Duyckaerts C, Frosch MP, Masliah E, Mirra SS, Nelson PT, Schneider JA, Thal DR, Thies B, Trojanowski JQ, Vinters HV, Montine TJ (2012) National Institute on Aging-Alzheimer's Association guidelines for the neuropathologic assessment of Alzheimer's disease. *Alzheimer's Dementia* **8**, 1-13.

[39] Bateman RJ, Xiong C, Benzinger TLS, Fagan AM, Goate A, Fox NC, Marcus DS, Cairns NJ, Xie X, Blazey TM, Holtzman DM, Santacruz A, Buckles V, Oliver A, Moulder K, Aisen PS, Ghetti B, Klunk WE, McDade E, Martins RN, Masters CL, Mayeux R, Ringman JM, Rossor MN, Schofield PR, Sperling RA, Salloway S, Morris JC (2012) Clinical and biomarker changes in dominantly inherited Alzheimer's disease. *New Engl J Med* **367**, 795-804.

[40] Maruyama M, Shimada H, Suhara T, Shinotoh H, Ji B, Maeda J, Zhang M-, Trojanowski J, Lee V-, Ono M, Masamoto K, Takano H, Sahara N, Iwata N, Okamura N, Furumoto S, Kudo Y, Chang Q, Saido T, Takashima A, Lewis J, Jang M-, Aoki I, Ito H, Higuchi M (2013) Imaging of tau pathology in a tauopathy mouse model and in alzheimer patients compared to normal controls. *Neuron* **79**, 1094-1108.

[41] Mangialasche F, Solomon A, Winblad B, Mecocci P, Kivipelto M (2010) Alzheimer's disease: clinical trials and drug development. *Lancet Neurol* **9**, 702-716.

[42] Kenigsberg P-, Aquino J-, Bérard A, Gzil F, Andrieu S, Banerjee S, Brémond F, Buée L, Cohen-Mansfield J, Mangialasche F, Platel H, Salmon E, Robert P (2016) Dementia beyond 2025: Knowledge and uncertainties. *Dementia* **15**, 6-21.

[43] Jankowsky JL, Zheng H (2017) Practical considerations for choosing a mouse model of Alzheimer's disease. *Mol Neurodegeneration* **12**.

[44] Hashimoto S, Ishii A, Kamano N, Watamura N, Saito T, Ohshima T, Yokosuka M, Saido TC (2018) Endoplasmic reticulum stress responses in mouse models of Alzheimer's disease: Overexpression paradigm versus knockin paradigm. *J Biol Chem* **293**, 3118-3125.

[45] Saito T, Matsuba Y, Yamazaki N, Hashimoto S, Saido TC (2016) Calpain activation in Alzheimer's model mice is an artifact of APP and presenilin overexpression. *J Neurosci* **36**, 9933-9936.

[46] Kraus A, Race B, Phillips K, Winkler C, Saturday G, Kurnellas M, Rothbard JB, Groveman BR, Steinman L, Caughey B (2016) Genetic background modulates outcome of therapeutic amyloid peptides in treatment of neuroinflammation. *J Neuroimmunol* **298**, 42-50.

[47] Wang X, Zhang C, Szábo G, Sun Q- (2013) Distribution of CaMKIIa expression in the brain in vivo, studied by CaMKIIa-GFP mice. *Brain Res* **1518**, 9-25.

[48] Cheng IH, Palop JJ, Esposito LA, Bien-Ly N, Yan F, Mucke L (2004) Aggressive amyloidosis in mice expressing human amyloid peptides with the Arctic mutation. *Nat Med* **10**, 1190-1192.

[49] Hernandez AL, Shah D, Craessaerts K, Saido T, Saito T, De Strooper B, Van der Linden A, D'Hooge R (2017) Subtle behavioral changes and increased prefrontal-hippocampal network synchronicity in APPNL-G-Fmice before prominent plaque deposition. *Behav Brain Res* .

[50] Brasnjevic I, Lardenoije R, Schmitz C, Van Der Kolk N, Dickstein DL, Takahashi H, Hof PR, Steinbusch HWM, Rutten BPF (2013) Region-specific neuron and synapse loss in the hippocampus of APPSL/PS1 knock-in mice. *Transl Neurosci* **4**, 8-19.

Figure 1 – Manuscript running title: 'Behaviour and histology in a novel *APP* knock-in mouse'

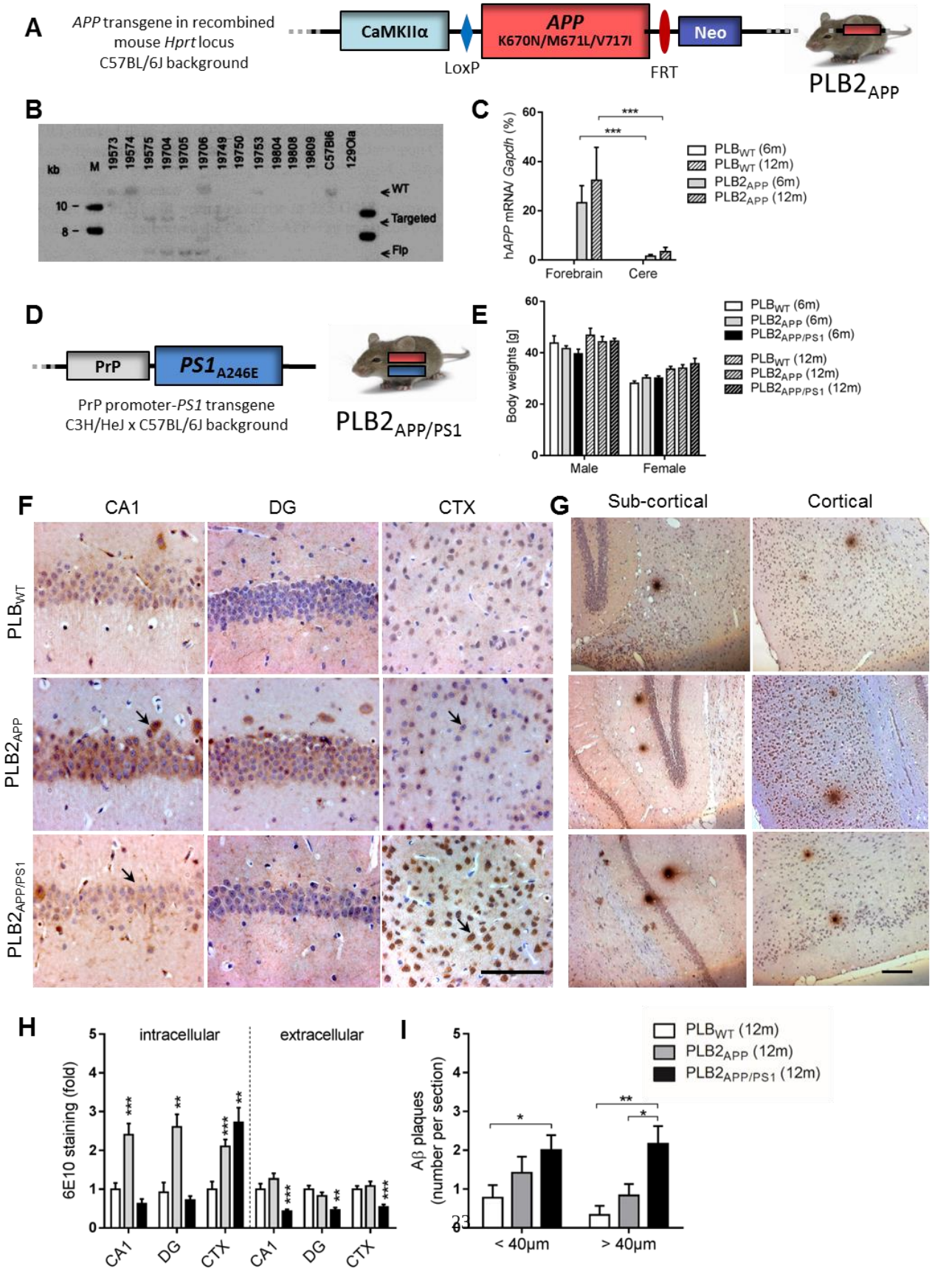

Figure 2 – Manuscript running title: 'Behaviour and histology in a novel *APP* knock-in mouse'

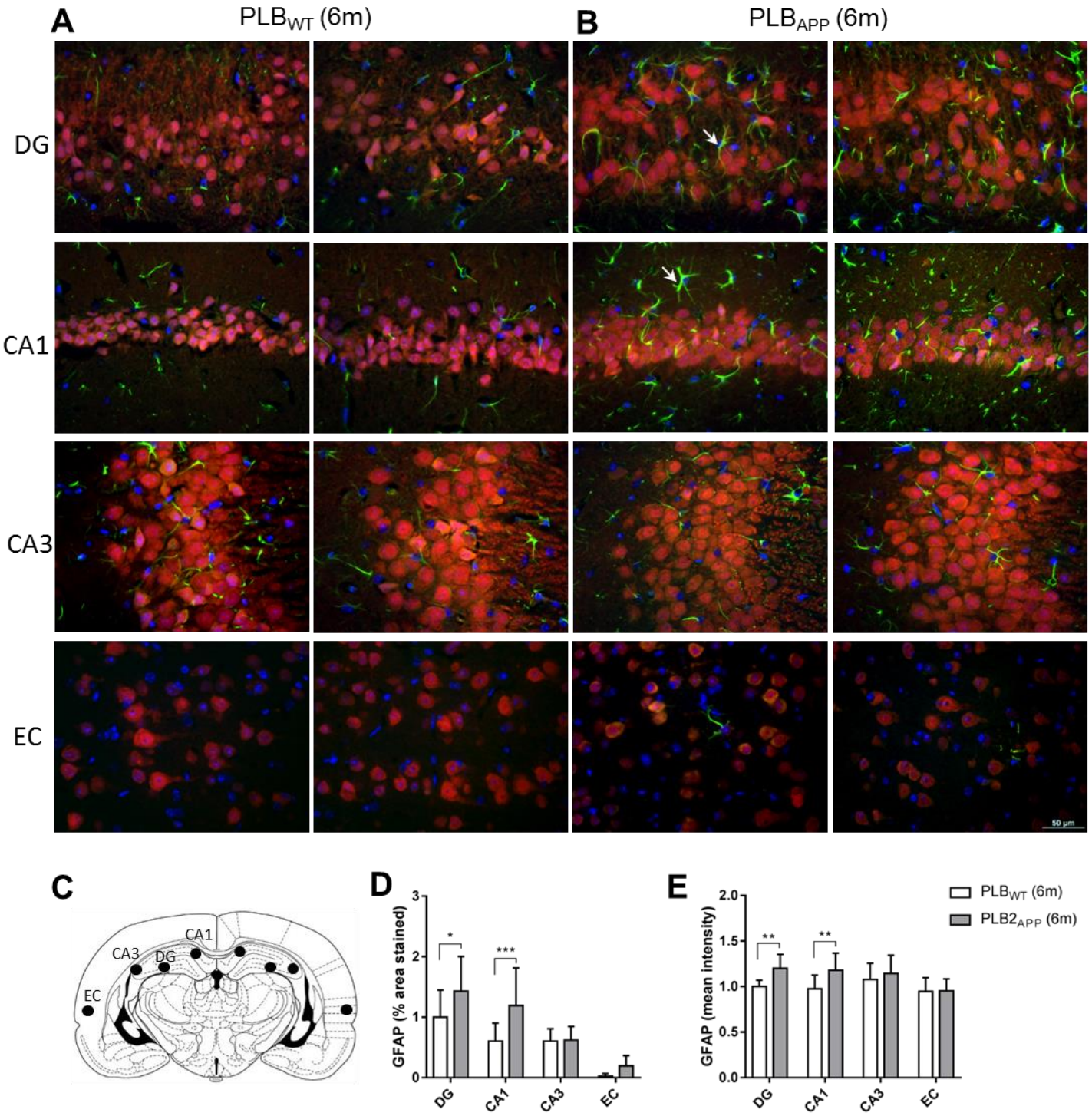

Figure 3 – Manuscript running title: 'Behaviour and histology in a novel *APP* knock-in mouse'

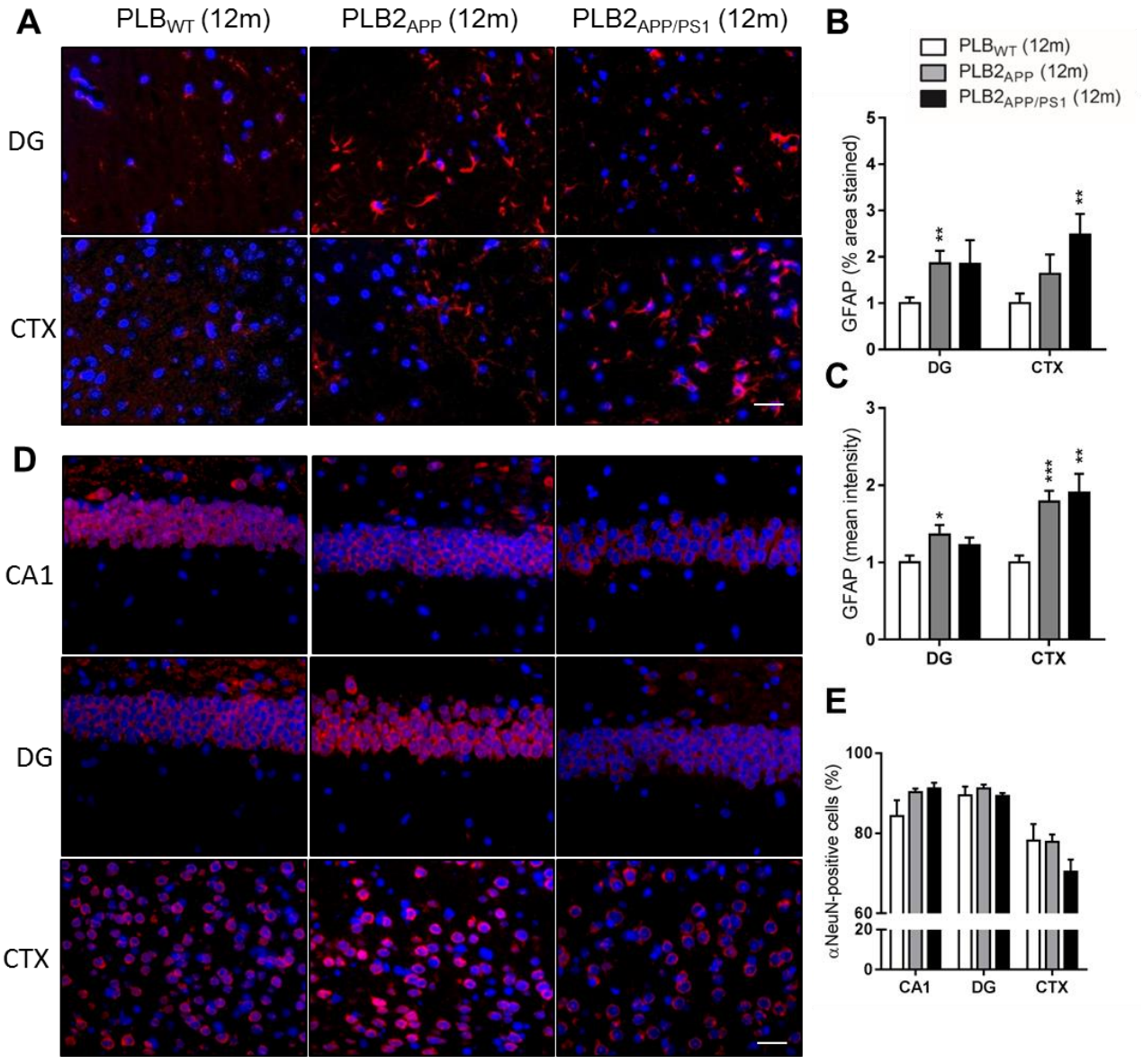

Figure 4 – Manuscript running title: 'Behaviour and histology in a novel *APP* knock-in mouse'

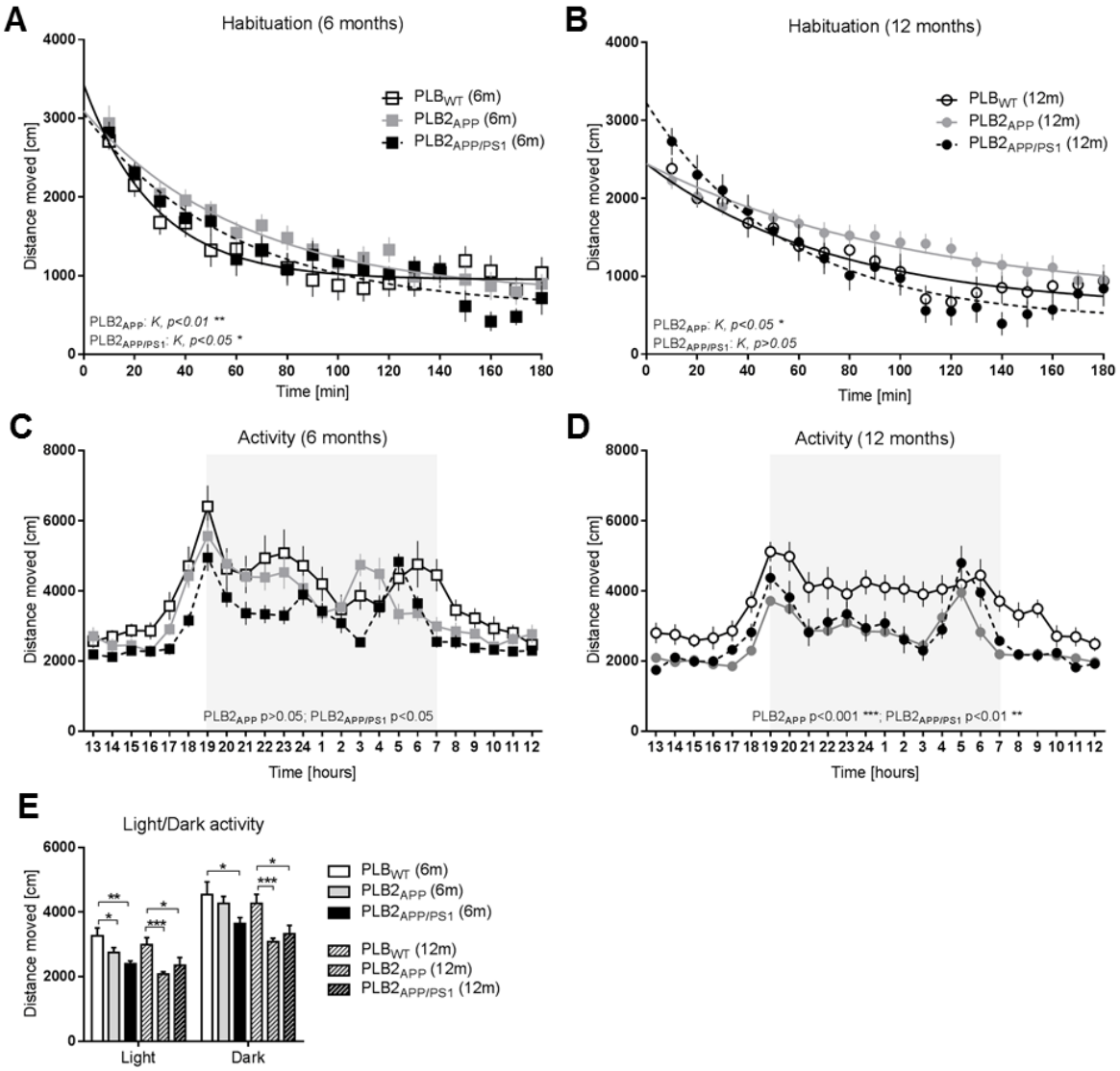

Figure 5 – Manuscript running title: 'Behaviour and histology in a novel *APP* knock-in mouse'

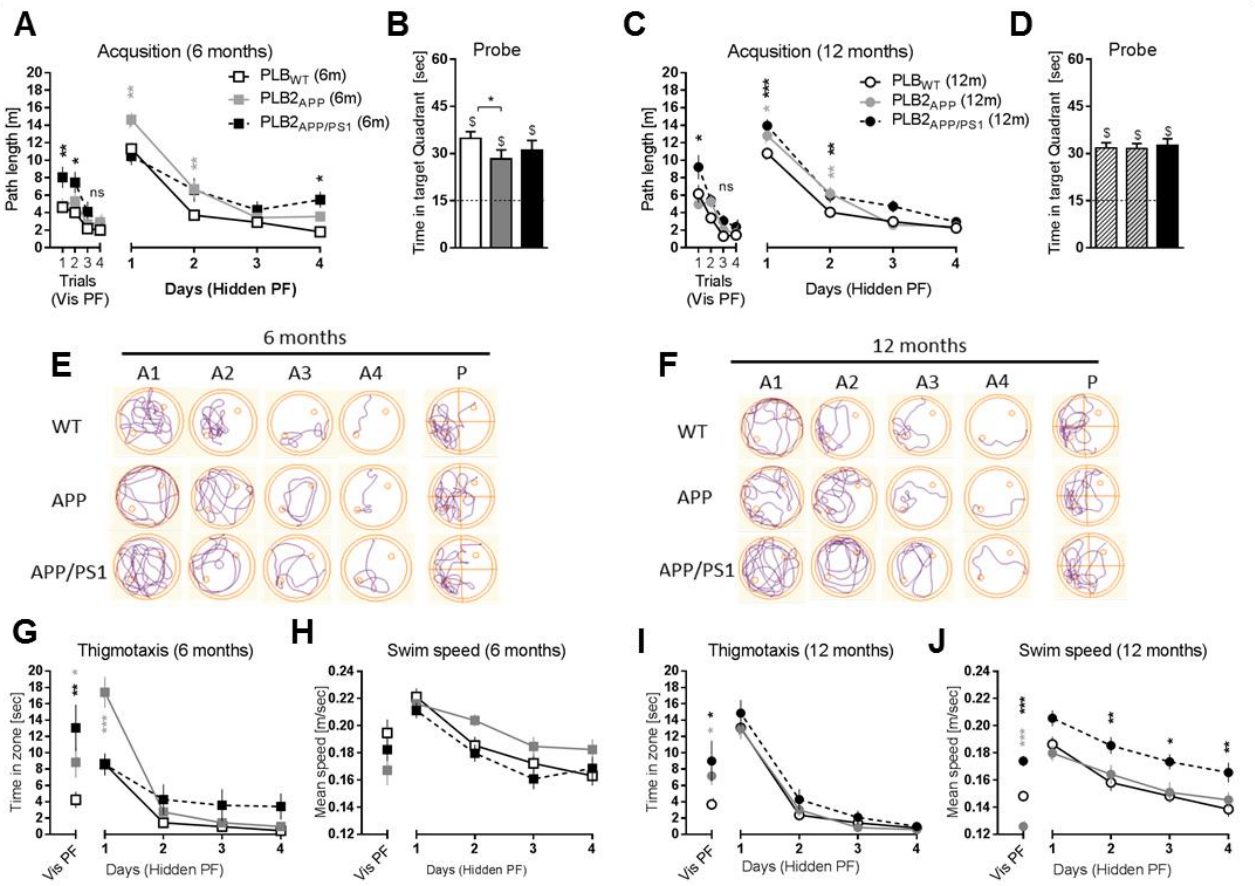

Figure 6 – Manuscript running title: 'Behaviour and histology in a novel *APP* knock-in mouse'

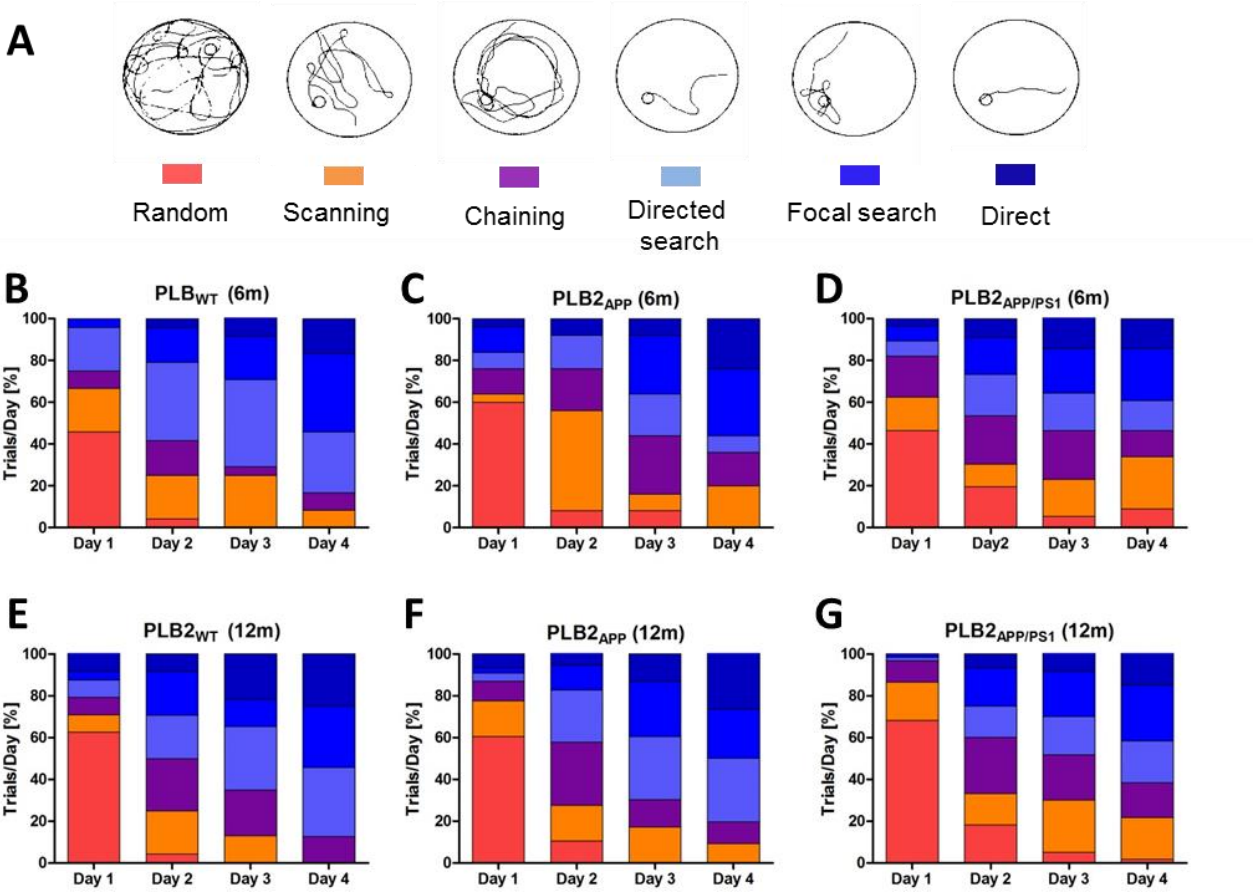

H

6m	WT vs. APP	WT vs APP/PS1	APP vs. APP/PS1
Day 1	χ^2= 28.0, df=10, p<0.01	χ^2= 17.6, df=10, p=0.06	χ^2= 12.4, df=10, p>0.05
Day 2	χ^2= 39.4, df=10, p<0.001	χ^2= 22.2, df=10, p<0.05	χ^2= 47.1, df=10, p<0.001
Day 3	χ^2= 43.6, df=10, p<0.001	χ^2= 30.7, df=10, p<0.001	χ^2= 7.7, df=10, p>0.05
Day 4	χ^2= 21.44, df=10, p<0.05	χ^2= 27.1, df=10, p<0.01	χ^2= 14.9, df=10, p>0.05
12m	**WT vs. APP**	**WT vs APP/PS1**	**APP vs. APP/PS1**
Day 1	χ^2= 4.8, df=10, p>0.05	χ^2= 16.5, df=10, p=0.08	χ^2= 8.3, df=10, p>0.05
Day 2	χ^2= 7.6, df=10, p>0.05	χ^2= 11.3, df=10, p>0.05	χ^2= 6.0, df=10, p>0.05
Day 3	χ^2= 9.5, df=10, p>0.05	χ^2= 20.6, df=10, p<0.05	χ^2= 13.3, df=10, p>0.05
Day 4	χ^2= 9.9, df=10, p>0.05	χ^2= 28.3, df=10, p<0.01	χ^2= 12.6, df=10, p>0.05